Enhancing Photocatalytic Activity of ZnO Nanoparticles in a Circulating Fluidized Bed with Plasma Jets

Shiwei Ma[1,#], Yunyun Huang[1,#], Ruoyu Hong[*], Xuesong Lu[2], Jianhua Li[3]

[1] *College of Chemical Engineering, Fuzhou University, Fuzhou 350108, China*

[2] *School of Engineering and Physical Sciences, Heriot-Watt University, Edinburgh EH14 4AS, UK*

[3] *Coal Chemical R & D Center of Kailuan Group, Tangshan 063611, China*

[*] *Corresponding author. E-mail address: rhong@fzu.edu.cn (R. Hong).*

[#] These authors contributed equally to this work

Abstract: In this work, zinc oxide (ZnO) nanoparticles were modified in a circulating fluidized bed through argon and hydrogen (Ar-H) alternative-current (AC) arc plasma, which shows the characteristics of non-equilibrium and equilibrium plasma at the same time. In addition, a circulating fluidized bed with two plasma jets was used for cyclic processing. The catalytic degradation performance on Rhodamine B (Rh B) by Ar-H plasma modified ZnO and pure ZnO was tested in aqueous media to identify the significant role of hydrogen atoms in Rh B degradation mechanism. Meanwhile, the effects of plasma treatment time on the morphology, size and photocatalytic performance of ZnO were also investigated. The results demonstrated that ZnO after 20 minutes-treatment by Ar-H plasma showed Rh B photocatalytic degradation rate is ten times greater than that of pure ZnO, and the reaction follows a first-kinetics for the Rh B degradation process. Furthermore, the photocatalyst cycle experiment curve exhibited that the modified ZnO still displays optimum photocatalytic activity after five cycles of experiment. The improvement of photocatalytic activity and luminescence performance attributes to the significant

increase of the surface area, and the introduction of hydrogen atoms on the surface also could

enhance the time of carrier existence where the hydrogen atoms act as shallow donors.

Key words: Plasma, zinc oxide, photocatalysis, nanomaterials.

1.   Introduction

The world environmental problems today are excessive pollution, waste of resources and

energy shortages. Semiconductor photocatalysis on waste or pollution treatments is a promising

environment-friendly and effective method. This technology makes full use of the semiconductor

photocatalysts through photoelectric chemistry to degrade organic pollutant molecules based on

the efficient use of solar energy[1-3].

Among various semiconductors, zinc oxide (ZnO) with the wide band gap (3.37 eV)[4], large

exciton blinding energy (60 meV)[5], good photoelectric properties, non-toxicity, abundance and

environmental stability[6,7] perform much better than other photocatalysts. Therefore, ZnO has

been widely researched for various applications including photocatalysts[8-10], chemical

sensors[11], transparent electrodes[12], solar cells[13] and luminescent materials[14,15]. Especially,

ZnO performs well on the photocatalytic. When ZnO is irradiated by the visible or ultraviolet light,

the electrons obtain light energy to transit from the valence band to the conduction band, and

generate electron-hole pairs. Simultaneously, some electrons return to the valence band in the

form of heat and light emission, and other carriers move on the ZnO surface. Among them,

electrons have strong reducibility, and photo-generated holes have strong oxidizing properties.

They further react with pollutants to achieve photocatalytic effects[16].

However, ZnO nanoparticles as photocatalyst also suffers several problems: (i) The bandgap of ZnO is too wide for electron transition, which makes it only respond to the ultraviolet region of sunlight[8], and the ultraviolet region only occupies a ratio of 5-7% sunlight. To expand the region of light response, modification of ZnO nanopowders is essential. (ii) The rapid recombination of electron-hole pairs in the catalytic process is also the main problem that seriously affects the photocatalytic performance[17-19]. To improve the photocatalytic performance of ZnO, it needs from two aspects to increase the absorption light threshold of ZnO and promote the effective separation of photogenerated carriers. Increasing the specific surface area and reducing the band gap were demonstrated to be effective methods to enhance the photocatalytic ability of ZnO. Several methods for modifying ZnO have been developed, such as metal element doping modification[20], non-metal element doping modification[21], semiconductor material composite loading[17,22], surface modification[23] and so on. However, these methods have disadvantages such as cumbersome preparation or serious post-treatment process or serious pollution of by-products, which limits the large-scale application of these methods[24].

Currently, plasma become a research hot point and has been extensively used in synthesis and modification of ZnO in recent years[25-27] because the high energy of the plasma could remove the surface state of the material, surface impurities or defects, and different plasmas would produce doping, deposition or reaction phenomena[26]. In particular, the arc plasma is highly valued due to combining the characteristics of non-equilibrium plasma and equilibrium plasma. Continuous modification of materials by arc plasma is a facile method of high yield[28].

Photocatalytic performance of ZnO depends on the modification conditions and methods[29].

Dao et al.[30]. modified ZnO thin films by Ar plasma and etching was observed on the surface. The grains on the surface were etched out, leading to a flatter surface with a smaller roughness. It suggested that the improvement of photoelectronic properties may be due to the effects of hydrogen ions produced by high-energy plasma ionized residual gases. Dev et al.[23]. and Baratto et al.[31]. reported similar improvements by Ar plasma treatment and proposed that the effects were attributed to incorporation of hydrogen. Nam et al.[26]. proposed the synthesis and modification methods of ZnO nanoparticles. No changes in specific surface area were observed, but oxygen was introduced into the ZnO surface, and O-H stretching peak was increased on the ZnO nanoparticles surface. The increase of free radicals is the main reason to enhance the photocatalytic performance. Nitrogen (N_2)[32] and ammonia (NH_3)[33] plasma treatment were also reported and they showed similar effect of the argon plasma.

In the previous work by research groups, the preparation method of zinc oxide[34] was studied, and modification methods such as aluminum doping[35] and Ar plasma[36] were also studied. In this article, based on previous research work, we combined plasma and fluidized bed to develop a more efficient, green and convenient new modification method.

In this study, ZnO nanoparticles were modified by Ar and Ar-H plasma, and factors on the photocatalytic performance were studied including output voltage, plasma treatment time and plasma types. We compared the photocatalytic activity of ZnO before and after modification and studied the mechanism of plasma to improve the photocatalytic performance. At the same time, the role of hydrogen irons in modification process was investigated. Finally, the ZnO nanoparticles with excellent photocatalytic ability were successfully obtained and applied.

## 2.   Materials and methods

2.1. Materials and apparatus

Argon (99.99%), hydrogen (99.99%) were purchased from Xinhang Industrial Gases Co. Ltd. (Fuzhou, China). AC high voltage power supply and transformer were obtained from Jiaxing Jialin Electronic Technology Co. Ltd. (open circuit voltage 20 kV, Jiaxing, China). Zinc oxide(ZnO) nanoparticles were obtained from Aladdin Co. (Shanghai, China).

Fig. 1 (a) shows plasma fluidized bed equipment used in the experiments, which is made up of stainless steel. It mainly consists of two compartments: (i) The plasma generator is composed of a pair of ceramic discharge nozzles (length 150 mm, inner diameter 40 mm) and two pairs of parallel electrodes (length 120 mm, bottom diameter 20 mm); (ii) The separation and collection units include cyclone separation, bag filter and induced draft fan. The fan helps the carrier gas to circulate the ZnO in the plasma reactor. The products are mainly collected by a cyclone separator, and the rest is collected after being separated from the exhaust gas through a cloth bag. The details on the facility are referred to Fig. 1 (a) and Table. 1 [37].
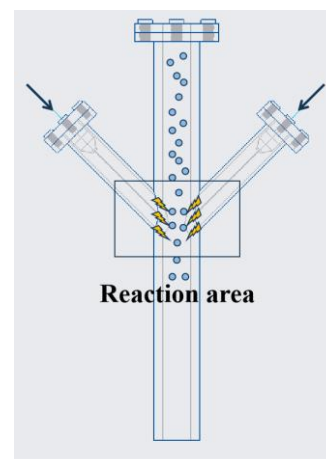
2.2. Modification process of ZnO

The modification process of ZnO nanoparticles by argon-hydrogen (Ar-H) arc plasma is shown in Fig. 1 (a) and the specific reaction area is shown in Fig. 1 (b). Firstly, the vacuum pump extracts the air from the reaction device to -0.1 M Pa. Then the induced draft fan was turned on to induce the Ar-H mixed gas into fluidized bed. When the AC power was supplied, the arc was generated between two parallel electrodes at the top region (as shown in the Fig. 1 (c)). The arc

discharged in the direction of the airflow in a yellow white color. With the Ar-H gas flow rate

increasing, the semicircular plasma beam enlarged and tended to be flame shape. At the same time,

the semicircular plasma beam became sparse and non-uniform as the arc was elongated. The

inhomogeneous arc was probably owing to the rough surfaces of the parallel electrodes. Finally,

when the arc remained stable, Ar and H_2 gas mixture was introduced in proportion into the plasma

reactor where the ratio and the gas flow rate were controlled and adjusted by a flow meter. The

plasma treatment time of ZnO were kept constant in five groups which were 30min, 60min, 90min,

120min and 150min and the corresponding products were denoted as T-1, T-2, T-3, T-4 and T-5,

respectively.

(a)
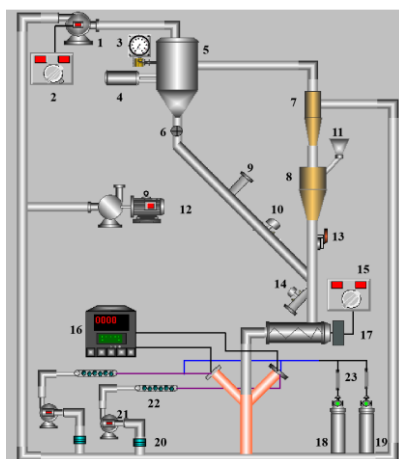
Reaction area

(b)

(c)

Fig. 1. (a) Schematic diagram of modification process device, (b) specific reaction area, (c) The plane of the AC sliding arc that occurs on the top of the flat electrode.

Table. 1. Detailed parts list

Part Number	Part Name	Part number	Part Name
1	Induced draft fan	12	Vacuum pump
2	Governor-1	13	Valve-2
3	Pressure gauge	14	Outlet
4	Blower	15	Governor-2
5	Bag separator	16	AC power
6	Rotary feeding valve	17	Screw propeller
7	Cyclone separator-1	18	Argon
8	Cyclone separator-2	19	Hydrogen
9	Oscillator	20	Filter membrane
10	Valve-1	21	Circulation pump
11	Feeding port	22	Desiccant
The diameter of all pipes in the device is 600mm		23	Flowmeter

2.3. Characterizations

The crystal structure of ZnO nanoparticles was investigated by X-ray diffraction (XRD) and the data were collected on DY1602/Empyrean equipped with Cu Kα radiation, using a step size of 0.2º and a counting time of 1 s per step in the range of 5-80º. The surface morphology of

plasma-treated ZnO nanoparticles was characterized by scanning electron microscopy (SEM, Verios G4 UC). PL spectra was used to observe luminous performance at room temperature. The specific surface area was measured by Brunauer Emmett Teller (BET). To investigate the photocatalytic capacity and optical performance of ZnO, the measurement by Ultraviolet-visble spectroscopy (UV-vis) was carried out in the range of 200-900 nm. The band gap and the photocatalytic reaction kinetic constant are calculated by UV diffuse reflectance, absorption spectra using the Kubelka-Munk method and the degradation curve of Rhodamine B, respectively. X-ray photoelectron spectroscopy (XPS) was used to characterize element differences before and after plasma treatment.

2.4. Measurement of photocatalytic abilities

The photocatalytic capacity of plasma-modified ZnO nanoparticles was investigated by degrading Rhodamine B (Rh B). In the experiments, 0.1 g of the modified samples was dispersed in 200 mL of Rh B aqueous solution (10 mM). Dark treatment of suspension was kept for 60 min until reaching adsorption and desorption equilibrium before illumination. Then the reaction was carried out at room temperature under a 50 W high-pressure mercury lamp with continuous cooling water. Before the irradiation, 4 mL of dye mixture was taken to centrifuge for every 10 minutes, and then the UV-vis was used to analysis supernatant at 554nm. Therefore, the photocatalytic degradation curves of Rh B solution were obtained, and the reaction type and kinetic constant of the degradation reaction of rhodamine B were calculated. The degradation percentages of Rh B solution were calculated using the formula C/C_0. The stability of the catalyst was also tested using cycle experiments.

3.   Results

3.1 XRD analysis of ZnO before and after modification

Fig. 2 shows the XRD patterns of ZnO before and after modification. The characteristic

diffraction peaks of the samples are 31.7º, 34.4º, 36.2º, 47.5º, 56.7º, 63.0º, 66.4º, 68.1º and 69.3º,

corresponding to the crystal planes of (100), (002), (101), (102), (110), (103), (200), (112) and

(201), respectively. This result is consistent with the diffraction peaks of hexagonal wurtzite phase

ZnO in the JCPDS standard card (No. 361451)[38]. As shown in Fig. 2, the Ar-H plasma treatment

resulted in a decrease in diffraction intensity, suggesting that the plasma treatment reduced the

crystallinity of ZnO nanoparticles and the plasma modification process did not just act on the
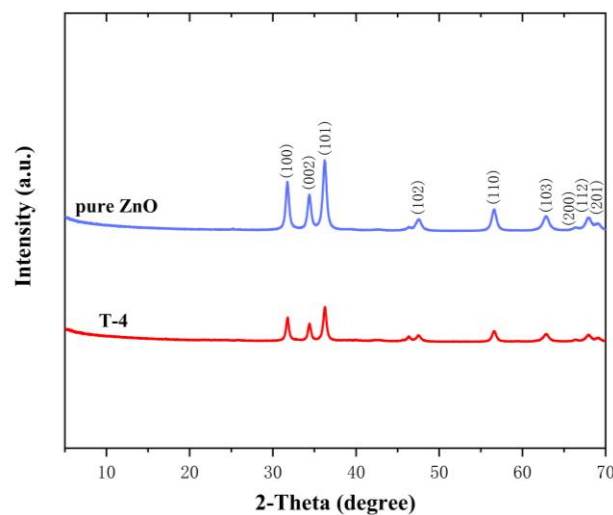
surface.

Fig. 2. XRD patterns of pure ZnO nanoparticles and T-4 sample.

Fig. 3. shows (002) and (100) XRD profiles of ZnO nanoparticles before and after 120 min

treatment. The (002) peak moved to a lower angle, while the (100) peak moved to a higher angle,

corresponding to an increase in the lattice constant c and a decrease in the lattice constant a,

respectively. These results mean that new ions/atoms are introduced at the crystal plane through

plasma treatment and modification, and the lattice united in the crystal grain block are stressed and

deformed. At the same time, it can also be proved that plasma acts not only on the surface but also
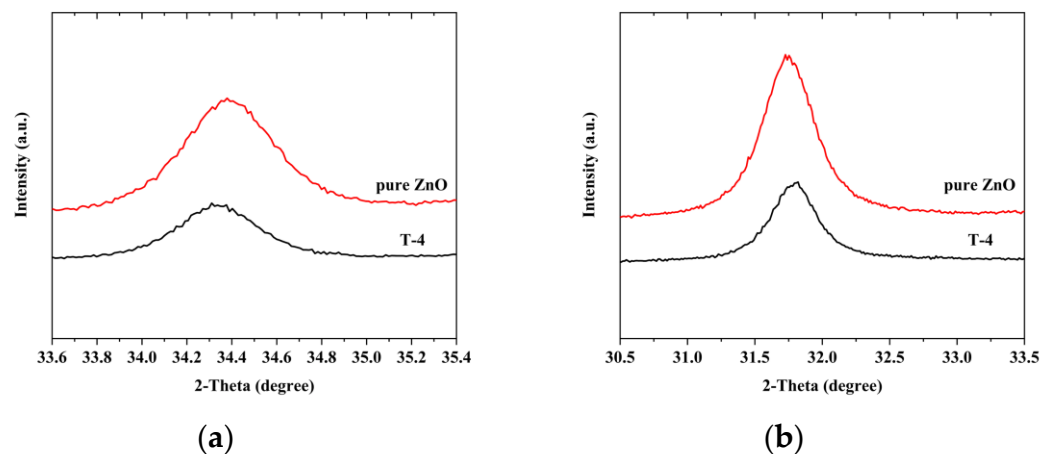
on the inside.

(a)   (b)

Fig. 3. Effect of the Ar-H plasma treatment time on the structural properties of the ZnO

nanoparticles. (a) Out-of-plane 002 and (b) in-plane 100 XRD.

3.2 SEM analysis of ZnO before and after modification

SEM images of original ZnO and T-4 samples are shown in Fig. 4 (a) and (b), respectively.

As shown in Fig. 4 (b), the pure ZnO shows a spherical agglomerated structure with a diameter of

100-800 nm. After 120 minutes of modification process, the etching and bombardment effects

were found on the surface of ZnO as well as a decrease in the degree of reunion, accompanied by

smoother surfaces and smaller roughness, as shown in Fig 4 (a). In theory, the improvement of

dispersibility and the reduction of nanoparticle size can effectively increase the specific surface

area of ZnO, thereby increasing the number of reactive sites and improving photocatalytic

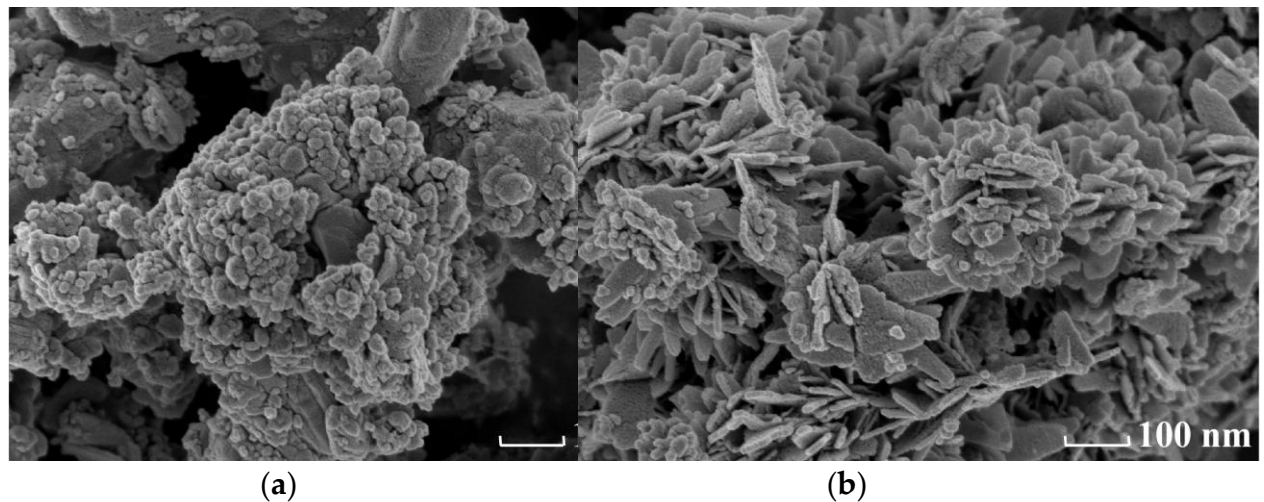efficiency. The specific verification can be observed from the BET test below.

Fig. 4. SEM images of products in different time, (a) 120min

plasma treatment (T-4 sample), (b) pure ZnO.

3.3 Characterization of specific surface area and carrier lifetime

Fig. 5 shows the changes in specific surface area and pore size distribution before and after

plasma modification of ZnO. As shown in Fig. 5 (a), the specific surface area of ZnO increased to

20.5630 m^2/g after 120 minutes of plasma treatment, which is 4.3 times higher than that of pure

ZnO. This may be due to the high energy of the plasma particles that etch the ZnO surface. The

increase of the specific surface area can provide more reaction active sites for the photocatalytic

reaction and improve the degradation efficiency. Fig. 5 (b) shows the pore size distribution curve

of the sample. It can be seen that the small pores of pure ZnO and T-4 are all distributed around 3

nm, and the large pores are all distributed between 15-30 nm. This porous structure is possibly

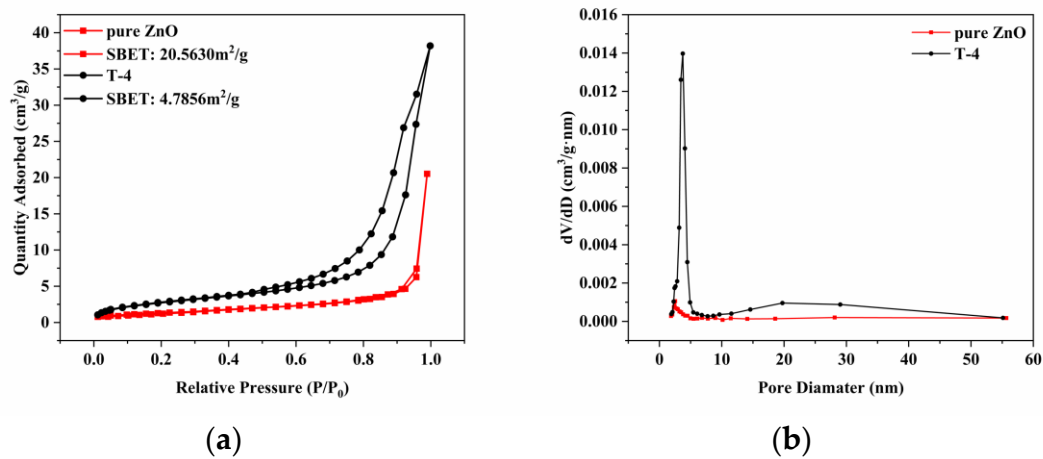caused by the gaps between small nanoparticles.

Fig. 5. (a) Nitrogen adsorption-desorption isotherms and (b) pore size distribution curves.

Photoluminescence spectrum (PL) was used to exam the luminescence intensity of ZnO and the recombination time of photogenerated electrons and holes. As shown in Fig. 6 (a), after plasma treatment, the luminescence intensity of ZnO at 380 nm decreased significantly, but the luminescence intensity increased at 500 nm. This may be due to the following two reasons:

(i) The recombination rate of photogenerated electrons and holes decreases, which leads to a decrease in luminescence intensity; (ii) The slight increase in luminous intensity at 500 nm may be related to the increase in oxygen vacancy concentration.

The carrier lifetime was shown in Fig. 6 (b) and (c). The carrier compound time of ZnO was changed from 194.4 ns to 251.5 ns, suggesting the photogenerated electron-hole recombination rate slowed down, which also proved the above conclusion.
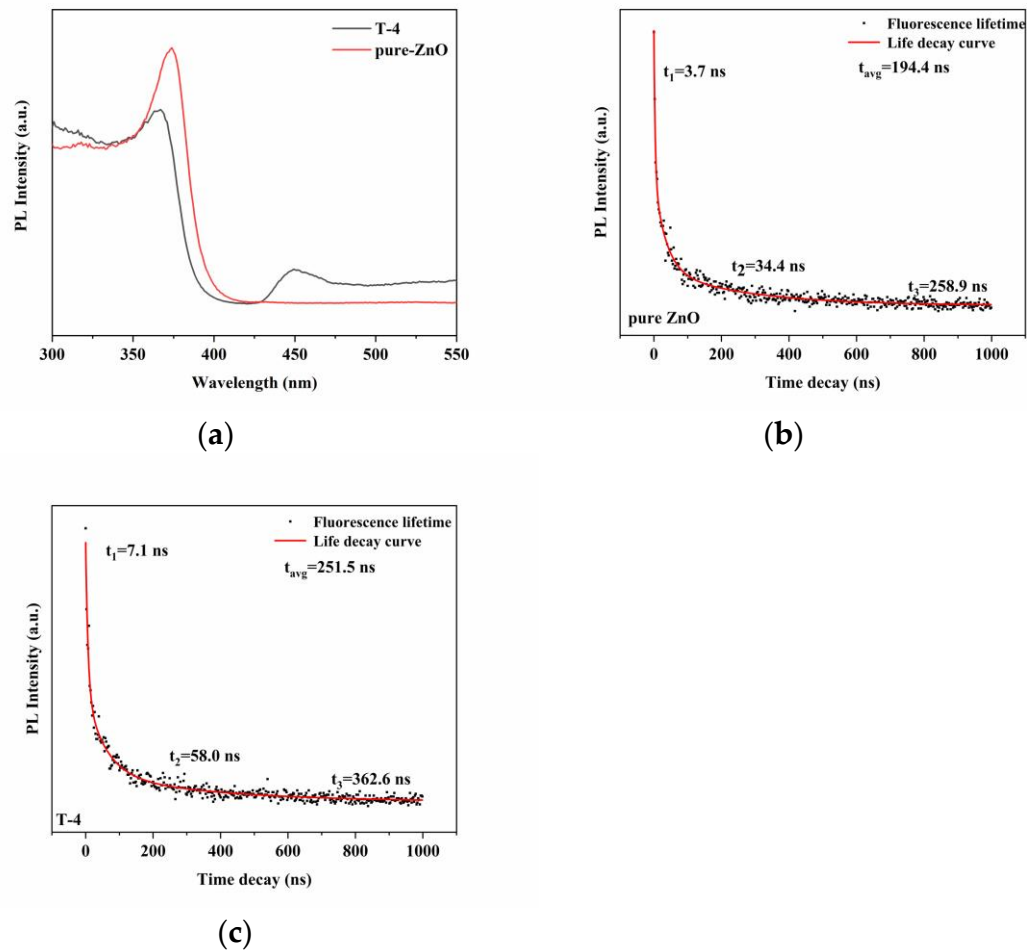
Fig. 6. (a) Photoluminescence spectra of ZnO and T-4, (b) Carrier lifetime curve of pure ZnO and

(c) Carrier lifetime curve of T-4 sample.

3.4 XPS analysis

X-ray electron spectroscopy (XPS) was used to evaluate the difference before and after Ar-H

plasma surface treatment. Fig. 7 (a) shows the XPS spectra for Zn 2p core level peaks, the Zn 2p

core energy peak shifted from 1022.6 eV to the binding energy region of 1021 eV. The results

display that the Zn on the surface of ZnO changes from oxygen-rich zinc before treatment to ZnO

containing metallic zinc after treatment. O 1s spectra is shown in Fig. 7 (b), it can be seen that the

main O 1s peaks of ZnO nanoparticles are fitted to the three peaks of 531.25 eV, 532.7 eV and

534.4 eV, corresponding to Zn-O, OH radicals and molecular water respectively. The shoulder peaks matching the OH radicals and molecular water increase significantly after plasma treatment and the peak intensity increased significantly, indicating that the chemical adsorption and physical adsorption of OH radicals and molecular water on the surface of ZnO are enhanced. Fig. 7 (c) shows the specific changes in the intensity of OH radicals and molecular water peaks before and after plasma treatment. The results show that Ar-H plasma treatment not only increases the concentration of OH radicals, but also has an effect on the surface adsorption of molecular water in the air which can cleave the double bond (C=N) to decompose the Rh B solution and couple with the N-H single bond of the Rh B solution, improving the photocatalytic effect effectively ultimately.
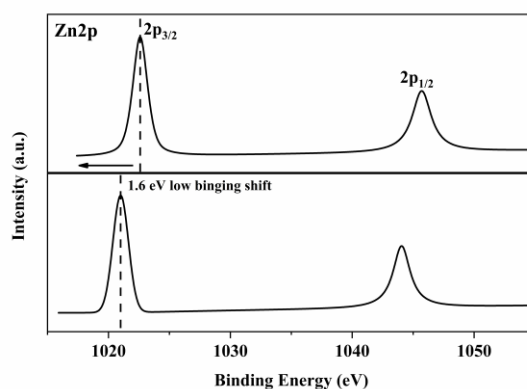
(a)
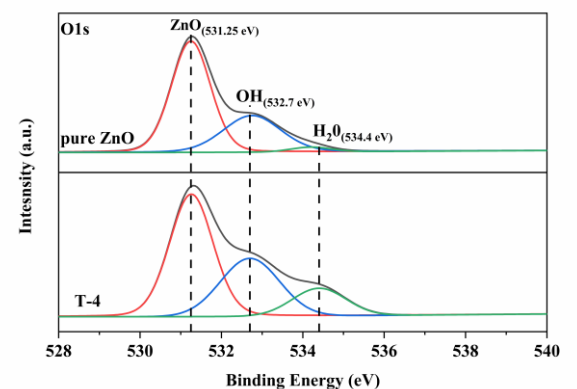
(b)
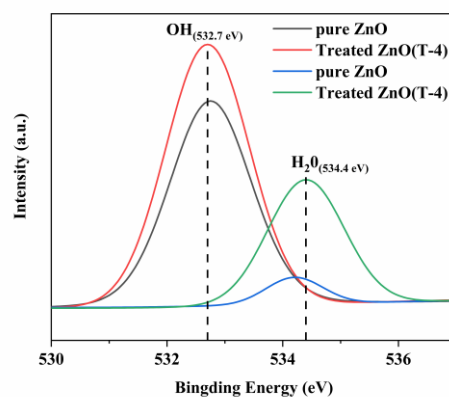
(c)

Fig. 7. Changes in XPS spectra of ZnO in the (a) Zn 2p, (b) O 1s peak and (c) OH and H_2O peaks

in O 1s regions before and after Ar-H plasma treatment.

3.5 Photocatalytic degradation of Rh B solution

To study the effect of treatment time on the activity of semiconductor catalysts, ZnO (T-1,

T-2, T-3. T-4, T-5) were used for photocatalytic degradation of Rh B solution. The experimentally

measured change curve of C/C_0 of Rh B solution with catalytic time is shown in Fig. 8 (a). The

blank experiment is the Rh B solution which is directly illuminated by a 50 W light source with no

catalyst. It is worth noting that ultraviolet light illumination in the absence of any photocatalyst or

dark conditions with catalysts do not lead to the photolysis of Rh B. In fact, in the blank

experiment, only 6.3% of the Rh B solution was degraded under the UV light source within 100

minutes. In the degradation experiment of adding pure ZnO, the degradation rate of Rh B was

improved but still showed poor degradation capacity. The Ar-H plasma modified ZnO

significantly enhanced the degradation of Rh B, and the degradation rate first increased and then

decreased with time. The degradation efficiency was the highest when the plasma treatment is 120

min, and the Rh B solution was degraded by 97.8% within 40 min.

The apparent enhancement in photocatalytic degradation capacity of ZnO nanoparticles could

be due to the effect of the increase in specific surface area (BET), decrease in electron-hole

recombination rate (PL), increase in surface OH radicals (XPS), and H atoms/ions as a shallow

donor. However, long-term plasma treatment time will cause the photocatalytic ability to decrease

(T-4), which may be attributed to the high energy of the plasma causing irreversible structural damage to the ZnO nanoparticles. In conclusion, the best modification time for plasma is 120min and the temporal evolution about the degradation of Rh B solution over T-4 was showed in Fig. 8 (b). The concentration of Rh B solution was indicated by the decrease in the intensity of the absorption peak.
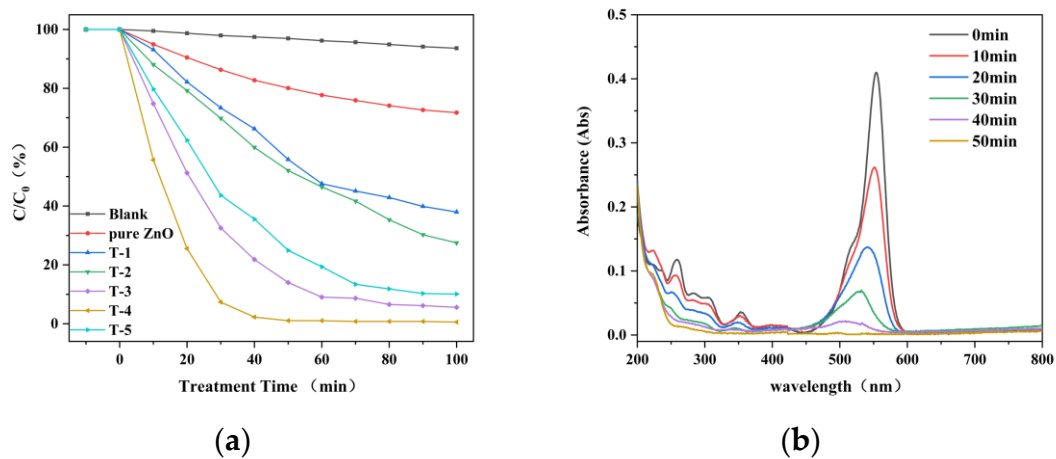

Fig. 8. (a) The Rh B concentration of different samples changes with time (b) The absorbance curve change with time when using T-4 product to degrade Rh B.

3.6 Photocatalytic degradation kinetics

The concentration of the solution can be calculated by measuring the light absorption intensity of the Rh B solution, according to the degradation efficiency of each catalyst based on the solution concentration. It is known through equation (1) fitting that the Rh B degradation process conforms to the first-order reaction kinetics:

$$- dC / dt = k \times C$$
$$- \ln(C / C_0) = k \times t \qquad (1)$$
$$\ln(C_0 / C) = k \times t$$

where, C, C_0, k, t represents the Rh B concentration of "t" time, the initial concentration of the dye, reaction rate constant (min^{-1}), the time at which photo catalytic degradation takes place, respectively.

Fitting the reaction kinetics of the results of each group of photocatalytic degradation experiments, the results are shown in Fig. 9. The degradation rate of Rh B solution decreased significantly after 90% degradation, so this experiment just performed a fitting analysis on the degradation rate before 90% degradation. It can be seen from the Fig. 9 that the reaction rate constant k in the blank experiment was only 0.00065 min^{-1}. After the catalyst was added, the degradation rate of Rh B was significantly increased, in which the reaction rate constant was 0.08933 min^{-1} when the treatment time was 120 min. The fitting data of the experimental results are shown in Table 2. In all the results, R^2 is greater than 0.99, indicating that $\ln(C_0/C)$ in the Rh B degradation experiment results shows a linear relationship with time t, which is a first-order reaction and meet the above equation. It can be seen that the sample with the best photocatalytic degradation effect on Rh B solution is T-4.
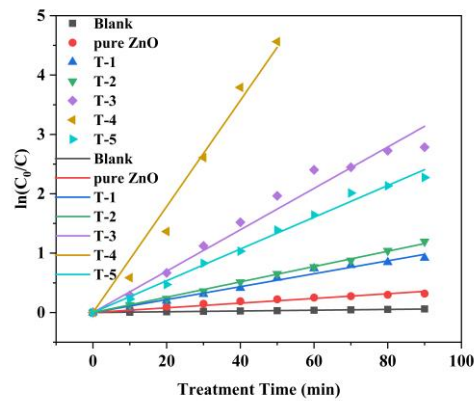

Fig. 9. The first-order reaction kinetics fitting curve of the degradation of Rh B in T4 sample.

Table 2. Degradation effect of samples with different plasma treatment time on Rh B solution

Sample	Degradation rate (%)	Reaction rate constant (min^{-1})	R^2
Blank	6.4	0.00065	0.999
Pure ZnO	28.3	0.00396	0.998
T-1	62.0	0.01089	0.994
T-2	72.5	0.01291	0.999
T-3	94.4	0.03485	0.991
T-4	99.4	0.08933	0.991
T-5	89.9	0.02675	0.997

To further study the mechanism of improving photocatalysis and the mechanism of plasma modification, more characterization methods were used. The ultraviolet visible diffuse reflectance spectroscopy (DRS) was used to characterize the degree of electron-hole pairs generated by the samples and the band gap width. The ultraviolet visible (UV) absorption edge wavelength was observed at the wavelength of 375 nm, which is the inherent absorption band gap of ZnO (3.2 eV) (shown in Fig. 10 (a)). The plasma modification process did not affect the change of the main absorption band of ZnO, the main absorption band of ZnO is shorter than 400 nm, and the absorption band of the T-4 sample was very similar to that of pure ZnO. T-4 sample also reveals other absorption peaks, which is due to plasma treatment in the visible light region (400-700 nm). T-4 nanomaterial exhibits a higher absorption rate, indicating that the sample also have a certain absorption capacity of solar photons in visible light.

The energy band theory provides a theoretical basis for the catalytic process of ZnO. As a typical semiconductor, the energy band of ZnO is split into two parts: the valence band and the conduction band. The valence band is usually occupied by electrons and exhibits lower energy, while the conduction band is empty and the energy is higher than the valence band. If the electron wants to transition from the valence band to the conduction band, it must pass through the band

gap between them, expressed by E_g[39]. The electron can successfully transit from the valence band to the conduction band only if the energy provided to the electron is not less than E_g.

When the energy of the incident light is not less than E_g, electrons will migrate from the valence band to the conduction band, and photo-generated electrons (e⁻) will be generated, and photo-generated holes (h⁺) will appear on the valence band. Some photogenerated electrons will consume energy to return to the valence band by luminescence or exotherm and recombine with photogenerated holes. Other photogenerated carriers are affected by the crystal defects and the surface energy state. The existence time of photogenerated carriers becomes longer, and they move to the surface of ZnO. The photogenerated electrons that reach the surface of ZnO have extremely strong reducibility, and the photogenerated holes have extremely strong oxidizing properties. They will react with water and oxygen on the surface of ZnO to generate various free radicals, such as: -OH, -O²⁻, etc. The generated free radicals will further react with pollutants and break the chemical bonds in their molecules to achieve the purpose of photocatalytic degradation. A smaller band gap theoretically means a stronger photocatalytic ability[39].

According to the Kubelka-Munk function[40], the band gap (E_g) is determined from the absorption spectra using equation as follows:

$$\alpha hv = A(hv - E_g)^{\eta} \tag{2}$$

where, α, h, v, A, Eg, η represents optical absorption coefficient, Planck constant, frequency of the incident photon, absorption constant for direct transition, band gap and index characterized by light absorption process, respectively. ZnO is a direct band gap semiconductor, so the value of η is 1/2. The values of α and A can be obtained according to the formula (3) and (4):

$$\alpha = A(1-R)^2 / 2R \tag{3}$$

$$A = -\lg(R) \tag{4}$$

where, R is the reflectance. As shown in Fig. 10 (b), the band gap was calculated by Eqs. (2) (3)

(4). The results showed that the band gap of ZnO was reduced from 3.22 eV to 2.99 eV after 120

min plasma modification process. Theoretically, the narrower the band gap, the easier it is to

generate carriers, which has a higher photocatalytic degradation efficiency. The possible reason is

that hydrogen acts as a shallow donor in ZnO, leading to a reduced band gap[30].

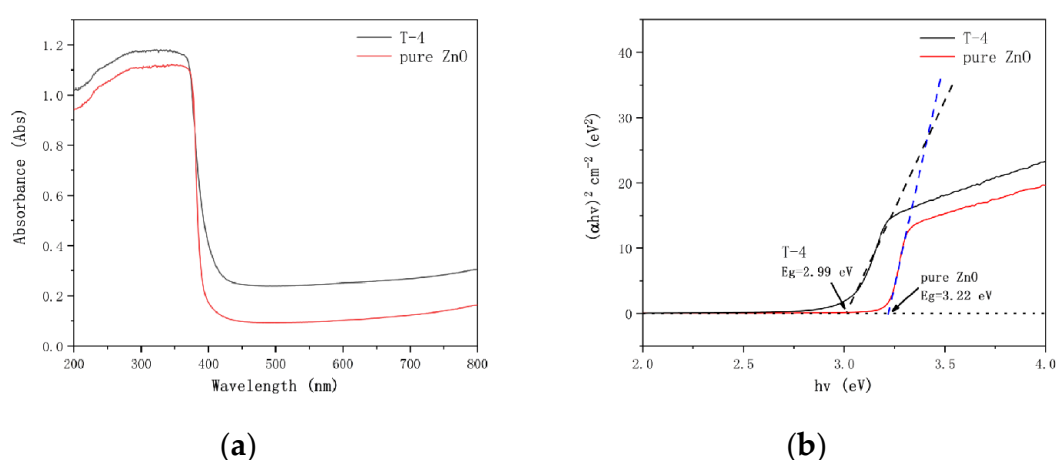

(a)   **(b)**

Fig. 10. (a) Ultraviolet-visible absorption spectrum and (b) the corresponding fitting curves and

the fitting result of the band gap.

3.7 Cycle experiment

The recyling of photocatalyst is of great significance to practical applications. When

evaluating the performance of a catalyst, stability is also an important indicator. The less the

catalytic efficiency decreases after the catalyst is recycled, the stronger the stability. Through five

repeated experiments under the same conditions, the stability of T-4 sample to the photocatalytic

degradation of Rh B solution was tested. As shown in Fig. 11 (a) and (b), the T-4 sample degraded

about 99.4% of Rh B in the first circle and the degradation efficiency of Rh B decreased to

89.76% within 100 minutes in the 5th cycle test. The reason for the decrease in photocatalytic

efficiency may be that the hydrogen element acting as a shallow donor is separated from ZnO during the cycle. In addition, the process of centrifugation, washing and drying will also cause sample loss, so it is reasonable to maintain a degradation rate close to 90% after 5 cycles.
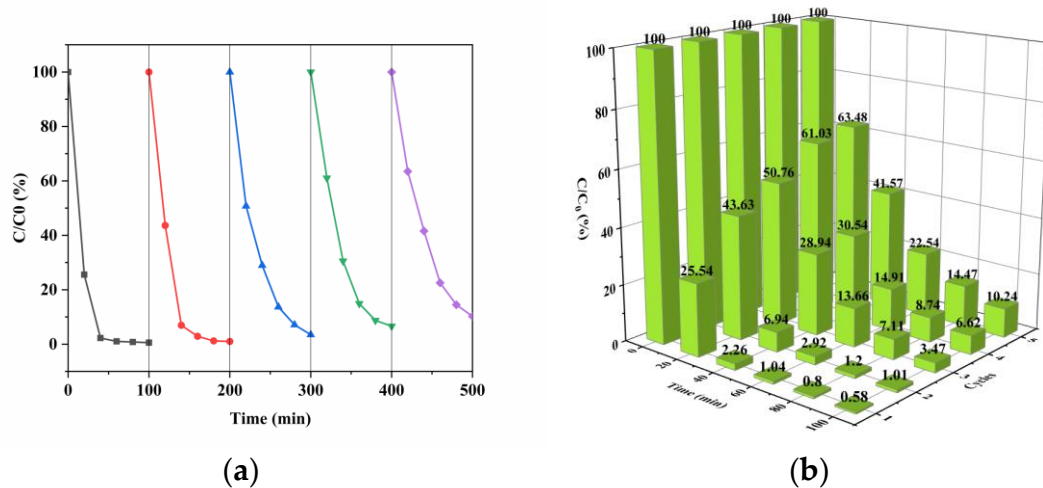

Fig. 11. (a) Cyclic degradation curve and (b) three-dimensional curve of Rh B.

4.   discussion

Based on the above analysis, the mechanism to improve the photocatalytic activity was speculated. The possible mechanism responsible for the increases in photocatalytic activity is due to oxygen vacancies produced by the etching of argon-hydrogen plasma[41-43]. Oxygen vacancies are considered to be one of the main defects generated by carriers in ZnO, and the increase in oxygen vacancies concentration will increase the photocatalytic activity of ZnO[44]. Firstly, the plasma particles have ultra-high energy, which can modify the surface of ZnO to produce some defects without changing the lattice structure. Then, hydrogen plasma can combine with oxygen to deepen the concentration of oxygen vacancies, theoretically. Another mechanism that leads to the improvement of photocatalytic performance may be resulted from hydrogen or hydrogen

incorporation acting as shallow donors. As shown in Fig. 12, hydrogen may also occupy

interstitial positions in the ZnO lattice and form impurity levels, which helps to increase the carrier

concentration. In addition, we also discussed the problem of photocatalytic performance

degradation caused by too long plasma modification. One possible explanation is that the ionized

impurities are scattered, when the modification time is extended and the concentration of

hydrogen ions reach a certain value, hydrogen will help the charge scattering[45,46]. On the other

hand, too long plasma modification time will damage the surface of the sample, generate

unsaturated dangling bonds and capture photo-generated electrons or holes[47]. These factors

ultimately reduce the number of reactive sites and the concentration of surface free radicals.
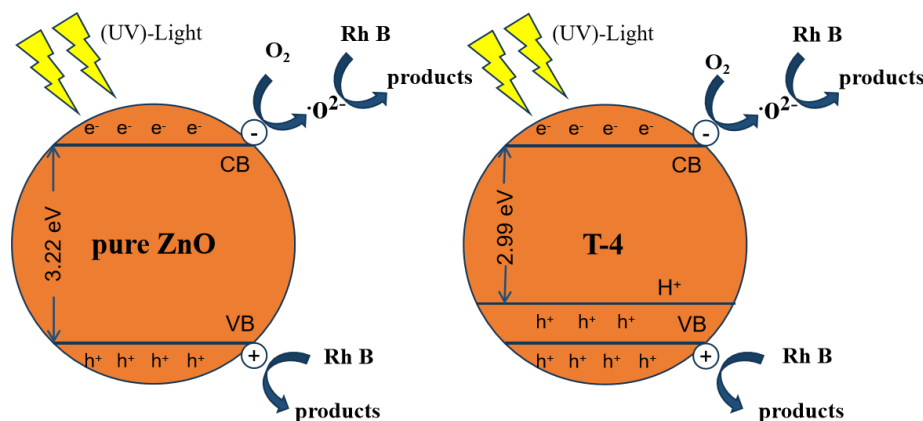

Fig. 12. Mechanism analysis of pure ZnO and T-4 sample.

5. Conclusions

In this work, a new process combining plasma and fluidized bed has been developed for the

modification of ZnO nanoparticles continuously using AC arc plasma. Compared with the

traditional plasma modification methods, the process has the advantages of simple operation and

continuous modification in large quantities. Under the optimal conditions of plasma modification

for 120 min, the band gap of ZnO was reduced to 2.99 eV, and the specific surface area was

increased to 20.5630 m^2/g. As the plasma treatment time increased, the photocatalytic efficiency of the sample first increased and then decreased, and the maximum degradation rate of Rh B solution was 0.08933 min^{-1} which was 22 times than that of unmodified ZnO. In addition, summation the characterization results of SEM, XPS, UV-vis, DRS and so on, the photocatalytic mechanism of modified ZnO was speculated. The Ar-H plasma treatment increased the specific surface area while reducing the band gap of ZnO, and an impurity level was formed in the band gap of ZnO by hydrogen elements, which was conducive to generate and transform photo-generated electron-hole pairs. Therefore, the plasma fluidized bed modified ZnO nanoparticles might provide a new idea to improve the application of ZnO photocatalysis.

Author Contributions: Conceptualization, Shiwei. Ma. and Ruoyu. Hong.; methodology, Shiwei. Ma.; software, Shiwei. Ma.; validation, Ruoyu. Hong., Yunyun. Huang. and Jianhua. Li.; formal analysis, Shiwei. Ma.; investigation, Shiwei. Ma.; resources, Shiwei. Ma.; data curation, Shiwei. Ma.; writing—original draft preparation, Shiwei. Ma.; writing—review and editing, Jianhua. Li. and Xuesong. Li.; visualization, Shiwei. Ma.; supervision, Yunyun. Huang.; project administration, Ruoyu. Hong.; funding acquisition, Ruoyu. Hong. And Yunyun. Huang. All authors have read and agreed to the published version of the manuscript.

830170771).

Conflicts of Interest: The authors declare no conflict of interest and all the authors approved the

manuscript for publication. The funders had no role in the design of the study; in the collection,

analyses, or interpretation of data; in the writing of the manuscript, or in the decision to publish

the results.

References

1.   Bazghale, A.A.; Mohammad-khah, A. Sonocatalytic decolorization of methylene blue from aqueous media by La:ZnO/GO nanocomposites. *Res Chem Intermediat* **2019**, *45*, 1985-2005.

2.   Sun, J.B.; Gu, Y.; Lu, X.W.; Si, L.; Zhang, Q.F. Hole Doping to Enhance the Photocatalytic Activity of Bi_4NbO_8Cl. *Catalysts* **2020**, *10*, 1425.

3.   Reichert, G.; Hilgert, S.; Fuchs, S.; Rodrigues Azevedo, J.C. Emerging contaminants and antibiotic resistance in the different environmental matrices of Latin America. *Environ Pollut* **2019**, *255*, 113140.

4.   Srikant, V.; Clarke, D.R. On the optical band gap of zinc oxide. *J Appl Phys* **1998**, *83*, 5447-5451.

5.   Teke, A.; Ozgur, U.; Dogan, S.; Gu, X.; Morkoc, H.; Nemeth, B.; Nause, J.; Everitt, H.O. Excitonic fine structure and recombination dynamics in single-crystalline ZnO. *Phys Rev B* **2004**, *70*, 195207.

6.   Xu, T.; Xie, C.S. Tetrapod-like nano-particle ZnO/acrylic resin composite and its multi-function property. *Prog Org Coat* **2003**, *46*, 297-301.

7.   Bhat, S.V.; Deepak, F.L. Tuning the bandgap of ZnO by substitution with Mn^{2+}, Co^{2+} and Ni^{2+}. *Solid State Commun* **2005**, *135*, 345-347.

8.   Luna-Flores, A.; Morales, M.A.; Agustin-Serrano, R.; Portillo, R.; Luna-Lopez, J.A.; Perez-Sanchez, G.F.; Hernandez-de la Luz, A.D.; Tepale, N. Improvement of the Photocatalytic Activity of ZnO/Burkeite Heterostructure Prepared by Combustion Method. *Catalysts* **2019**, *9*, 817.

9.   Franco, P.; Sacco, O.; De Marco, I.; Vaiano, V. Zinc Oxide Nanoparticles Obtained by Supercritical Antisolvent Precipitation for the Photocatalytic Degradation of Crystal Violet Dye. *Catalysts* **2019**, *9*, 346.

10.   Al-Fori, M.; Dobretsov, S.; Myint, M.T.Z.; Dutta, J. Antifouling properties of zinc oxide nanorod coatings. *Biofouling* **2014**, *30*, 871-882.

11.   Paliwal, A.; Sharma, A.; Tomar, M.; Gupta, V. Carbon monoxide (CO) optical gas sensor based on ZnO thin films. *Sensor Actuat B-Chem* **2017**, *250*, 679-685.

12.   Chen, S.; Wang, S. ZnO:H indium-free transparent conductive electrodes for active-matrix display applications. *Appl Phys Lett* **2014**, *105*, 223304.

13.   Rahman, M.; Wei, M.; Xie, F.; Khan, M. Efficient Dye-Sensitized Solar Cells Composed of Nanostructural ZnO Doped with Ti. *Catalysts* **2019**, *9,* 273.

14.   Vanheusden, K.; Warren, W.L.; Seager, C.H.; Tallant, D.R.; Voigt, J.A.; Gnade, B.E. Mechanisms behind green photoluminescence in ZnO phosphor powders. *J Appl Phys* **1996**, *79*, 7983-7990.

15.   Meyer, B.K.; Alves, H.; Hofmann, D.M.; Kriegseis, W.; Forster, D.; Bertram, F.; Christen, J.; Hoffmann, A.; Strassburg, M.; Dworzak, M. Bound exciton and donor-acceptor pair recombinations in ZnO. *Phys Status Solidi B* **2004**, *241*, 231-260.

16.   Behnajady, M.A.; Modirshahla, N.; Hamzavi, R. Kinetic study on photocatalytic degradation of CI Acid Yellow 23 by ZnO photocatalyst. *J Hazard Mater* **2006**, *133*, 226-232.

17.   Linsebigler, A.L.; Lu, G.Q.; Yates, J.T. Photocatalysis on TiO_2 surfaces-principles, mechanisms, and selected results. *Chem Rev* **1995**, *95*, 735-758.

18.   Han, W.; Ren, L.; Qi, X.; Liu, Y.; Wei, X.; Huang, Z.; Zhong, J. Synthesis of CdS/ZnO/graphene composite with high-efficiency photoelectrochemical activities under solar radiation. *Appl Surf Sci* **2014**, *299*, 12-18.

19.   Chen, D.; Wang, K.; Ren, T.; Ding, H.; Zhu, Y. Synthesis and characterization of the ZnO/mpg-C_3N_4 heterojunction photocatalyst with enhanced visible light photoactivity. *Dalton T* **2014**, *43*, 13105-13114.

20.   Kumar, P.S.; Selvakumar, M.; Bhagabati, P.; Bharathi, B.; Karuthapandian, S.; Balakumar, S. CdO/ZnO nanohybrids: facile synthesis and morphologically enhanced photocatalytic performance. *Rsc Adv* **2014**, *4*, 32977-32986.

21.   Liang, P.; Zhang, C.; Sun, H.; Liu, S.; Tade, M.; Wang, S. Photocatalysis of C, N-doped ZnO derived from ZIF-8 for dye degradation and water oxidation. *Rsc Adv* **2016**, *6*, 95903-95909.

22.   Anirudhan, T.S.; Deepa, J.R. Nano-zinc oxide incorporated graphene oxide/nanocellulose composite for the adsorption and photo catalytic degradation of ciprofloxacin hydrochloride from aqueous solutions. *J Clloid Interf Sci* **2017**, *490*, 343-356.

23.   Dev, A.; Niepelt, R.; Richters, J.P.; Ronning, C.; Voss, T. Stable enhancement of near-band-edge emission of ZnO nanowires by hydrogen incorporation. *Nanotechnology* **2010**, *21,* 065709.

24.   Qin, B.; Zhang, T.; Chen, H.; Ma, Y. The growth mechanism of few-layer graphene in the arc discharge process. *Carbon* **2016**, *102*, 494-498.

25.   Chen, C.; Lu, Y.; He, H.; Xiao, M.; Wang, Z.; Chen, L.; Ye, Z. Violet Emission in ZnO Nanorods Treated with High-Energy Hydrogen Plasma. *ACS Appl Mater Inter* **2013**, *5*, 10274-10279.

26.   Nam, S.H.; Boo, J.H. Enhancement of photocatalytic activity of synthesized ZnO nanoparticles with oxygen plasma treatment. *Catal Today* **2016**, *265*, 84-89.

27.   Chen, H.; Sun, Q.; Tian, T.; Zheng, L.; Barre, M.; Monot-Laffez, I.; Makowska-Janusik, M.; Li, G.; Kassiba, A.H. Defects and microstructure of highly conducting Al-doped ZnO ceramics obtained via spark plasma sintering. *J Eur Ceram Soc* **2020**, *40*, 5529-5534.

28.   Lee, D.H.; Kim, K.T.; Cha, M.S.; Song, Y.H. Optimization scheme of a rotating gliding

arc reactor for partial oxidation of methane. *P Combust Inst* **2007**, *31*, 3343-3351.

29. Gaspar, D.; Pereira, L.; Gehrke, K.; Galler, B.; Fortunato, E.; Martins, R. High mobility hydrogenated zinc oxide thin films. *Sol Energ Mat Sol C* **2017**, *163*, 255-262.

30. Dao, H.T.; Makino, H. Enhancement in optoelectrical properties of polycrystalline ZnO thin films by Ar plasma. *Mat Sci Semicon Proc* **2019**, *96*, 46-52.

31. Baratto, C.; Comini, E.; Ferroni, M.; Faglia, G.; Sberveglieri, G. Plasma-induced enhancement of UV photoluminescence in ZnO nanowires. *Crystengcomm* **2013**, *15*, 7981-7986.

32. Rodrigues, J.; Holz, T.; Allah, R.F.; Gonzalez, D.; Ben, T.; Correia, M.R.; Monteiro, T.; Costa, F.M. Effect of N_2 and H_2 plasma treatments on band edge emission of ZnO microrods. *Sci Rep-UK* **2015**, *5*, 10783.

33. Haye, E.; Job, N.; Wang, Y.; Penninckx, S.; Stergiopoulos, V.; Tumanov, N.; Cardinal, M.; Busby, Y.; Colomer, J.F.; Su, B.L. ZnO/Carbon xerogel photocatalysts by low-pressure plasma treatment, the role of the carbon substrate and its plasma functionalization. *J Colloid Interf Sci* **2020**, *570*, 312-321.

34. Zhang, P.; Hong, R.Y.; Chen, Q.; Feng, W.G.; Badami, D. Aluminum-doped zinc oxide powders: synthesis, properties and application. *J Mater Sci-Mater El* **2014**, *25*, 678-692.

35. Zhang, P.; Hong, R.Y.; Chen, Q.; Feng, W.G. On the electrical conductivity and photocatalytic activity of aluminum-doped zinc oxide. *Powder Technol* **2014**, *253*, 360-367.

36. Wang, X.; Zhang, P.; Hong, R. Preparation and application of aluminum-doped zinc oxide powders via precipitation and plasma processing method. *J Appl Polym Sci* **2015**, *132*, 215123.

37. Wang, F.; Hong, R. Continuous preparation of structure-controlled carbon nanoparticle via arc plasma and the reinforcement of polymeric composites. *Chem Eng J* **2017**, *328*, 1098-1111.

38. Omri, K.; Bettaibi, A.; Khirouni, K.; El Mir, L. The optoelectronic properties and role of Cu concentration on the structural and electrical properties of Cu doped ZnO nanoparticles. *Physica B* **2018**, *537*, 167-175.

39. Ye, C.; Bando, Y.; Shen, G.; Golberg, D. Thickness-dependent photocatalytic performance of ZnO nanoplatelets. *J Phys Chem B* **2006**, *110*, 15146-15151.

40. Sivakarthik, P.; Thangaraj, V.; Parthibavarman, M. A facile and one-pot synthesis of pure and transition metals (M=Co&Ni) doped WO_3 nanoparticles for enhanced photocatalytic performance. *J Mater Sci-Mater El* **2017**, *28*, 5990-5996.

41. Kim, W.; Bang, J.-H.; Uhm, H.S.; Lee, S.H.; Park, J.S. Effects of post plasma treatment on material properties and device characteristics in indium zinc oxide thin film transistors. *Thin Solid Films* **2010**, *519*, 1573-1577.

42. Kang, J.H.; Cho, E.N.; Kim, C.E.; Lee, M.J.; Lee, S.J.; Myoung, J.M.; Yun, I. Mobility enhancement in amorphous InGaZnO thin-film transistors by Ar plasma treatment. *Appl Phys Lett* **2013**, *102*, 22-32.

43. Jeong, B.-J.; Jeong, J.K.; Song, Y.M.; Lee, H.D.; Choi, H.S.; Lee, G.W. Mobility Improvement of Amorphous Indium-gallium- zinc Oxide Thin Film Transistor by Roll-to-roll Compatible Plasma Treatment. *J Semicond Tech Sci* **2020**, *20*, 163-169.

44. Akopyan, I.K.; Labzovskaya, M.E.; Lisachenko, A.A.; Novikov, B.V.; Serov, A.Y.; Titov,

V.V.; Filosofov, N.G. Manifestation of oxygen desorption in photoluminescence spectra of ZnO. *Phys Solid State+* **2016**, *58*, 1767-1771.

45. Kim, W.M.; Kim, Y.H.; Kim, J.S.; Jeong, J.; Baik, Y.J.; Park, J.K.; Lee, K.S.; Seong, T.Y. Hydrogen in polycrystalline ZnO thin films. *J Phys D Appl Phys* **2010**, *43*, 365406.

46. Takahashi, I.; Hayashi, Y. Synthesis of hydrogen-doped zinc oxide transparent conductive films by RF magnetron sputtering. *JPN J Appl Phys* **2015**, *54*, 01AD07.

47. Kim, H.R.; Lee, G.H.; Kim, D.H. Effects of hydrogen plasma treatment on the structural and electrical properties of sputter-deposited SnO2 thin films. *J Phy D Appl Phys* **2011**, *44*, 185203.